Temperature Dependences for the Reactions of O^- and O_2^- with $O_2(a^1\Delta_g)$ from 200 to 700 K

Anthony Midey,[†,‡] Itzhak Dotan,[†,§] and A. A. Viggiano*[,†]

Air Force Research Laboratory, Space Vehicles Directorate, 29 Randolph Road, Hanscom Air Force Base, Massachusetts 01731-3010, and Open University of Israel, 108 Ravutski Street, Raanana, Israel 43107

Received: November 1, 2007; In Final Form: January 15, 2008

Rate constants and product ion distributions for the O^- and O_2^- reactions with $O_2(a\ ^1\Delta_g)$ were measured as a function of temperature from 200 to 700 K. The measurements were made in a selected ion flow tube (SIFT) using a newly calibrated $O_2(a\ ^1\Delta_g)$ emission detection scheme with a chemical singlet oxygen generator. The rate constant for the O_2^- reaction is $\sim 7 \times 10^{-10}$ cm^3 s^{-1} at all temperatures, approaching the Langevin collision rate constant. Electron detachment was the only product observed with O_2^-. The O^- reaction shows a positive temperature dependence in the rate constant from 200 to 700 K. The product branching ratios show that almost all of the products at 200 K are electron detachment, with an increasing contribution from the slightly endothermic charge-transfer channel up to 700 K, accounting for 75% of the products at that temperature. The increase in the overall rate constant can be attributed to this increase in the contribution the endothermic channel. The charge-transfer product channel rate constant follows the Arrhenius form, and the detachment product channel rate constant is essentially independent of temperature with a value of $\sim 6.1 \times 10^{-11}$ cm^3 s^{-1}.

Introduction

Reactions of O_2^- and O^- with $O_2(a^1\Delta_g)$ are important for a variety of systems. In the D-region of the ionosphere, the conversion of ions into electrons via reactions 1 and 2a affects

$$O_2^- + O_2(a^1\Delta_g) \rightarrow 2O_2 + e + 52\ \text{kJ mol}^{-1} \quad (1)$$

$$O^- + O_2(a^1\Delta_g) \rightarrow O_3 + e + 60\ \text{kJ mol}^{-1} \quad (2a)$$

$$O^- + O_2(a^1\Delta_g) \rightarrow O_2^- + O - 3\ \text{kJ mol}^{-1} \quad (2b)$$

the equilibrium electron concentration, which, in turn, controls radiowave propagation because electrons interact with the radiowaves and ions essentially do not.[1] Further interest in these $O_2(a^1\Delta_g)$ reactions has developed because of their importance in the electric oxygen−iodine laser (EOIL) system. In this system, the atomic iodine laser transition at 1315 nm, $I(^2P_{1/2} \rightarrow {}^2P_{3/2})$, is excited by energy transfer to atomic iodine from $O_2(a^1\Delta_g)$ that is produced in an electric discharge on oxygen and helium.[2−6] O^- is readily formed in such discharges by dissociative attachment of electrons to O_2; thus, electron detachment via reaction 2a helps to sustain the discharge.[7,8] Beyond this practical importance, reaction 1 is the only known example of Penning detachment.[9] This process is the negative ion analogue of the familiar Penning ionization process between a metastable neutral and another neutral. In Penning detachment, electronic energy from the metastable neutral collision partner is used to detach an electron from an ion.

Given the relevance of reactions 1 and 2, two direct measurements of the rate constants for these reactions have been made previously[10,11] and two additional determinations of the rate constant for reaction 2 have been obtained by extensive modeling of complicated plasmas.[12,13] The thermochemistry shown for reactions 1 and 2 has been calculated from the NIST Webbook values.[14] Recently, we have remeasured the kinetics for reactions 1 and 2 in a selected ion flow tube (SIFT) for the reactions of O_2^- and O^- with $O_2(a^1\Delta_g)$ at 300 K.[15] The rate constant for reaction 1 has been found to be substantially larger than previous measurements,[10,11] and the rate constant for reaction 2 is considerably smaller. The presence of channel 2b has been detected for the first time, reflecting the advantages of using a SIFT instead of a flowing afterglow. In all of the previous direct experiments,[10,11] $O_2(a^1\Delta_g)$ was generated in a microwave discharge on O_2.

Our recent measurements also used the microwave discharge technique to generate $O_2(a^1\Delta_g)$.[15] In that work, the $O_2(a^1\Delta_g)$ concentration in the SIFT was measured by calibrating a newly designed emission detection scheme to an absolute standard. Unfortunately, O atoms are an unwanted byproduct of the discharge method and they also react with both O_2^- and O^-. Passing the discharge effluent over glass wool with a mercury oxide coating effectively quenches O atoms and has been used in the earlier measurements.[10,11] However, given the current environmental restrictions on mercury use, ridding the flow stream of atomic oxygen has proven difficult. Consequently, corrections to the recent SIFT data were made for small concentrations of the O impurity, and to a lesser extent for an O_3 impurity, that could not be completely removed. These corrections are relatively small for the faster O_2^- reaction, but they are more substantial for the slower O^- reaction.[15]

Studying temperature dependences has been prohibitive because of the complications from O atoms. Therefore, we have adapted a chemical singlet oxygen generating technique to create

* Corresponding author. E-mail: AFRL.RVB.PA@hanscom.af.mil.
† Air Force Research Laboratory.
‡ Under contract to the Institute for Scientific Research, Boston College, Chestnut Hill, MA 02467.
§ Open University of Israel.

10.1021/jp710539s CCC: $40.75
Published on Web 03/11/2008

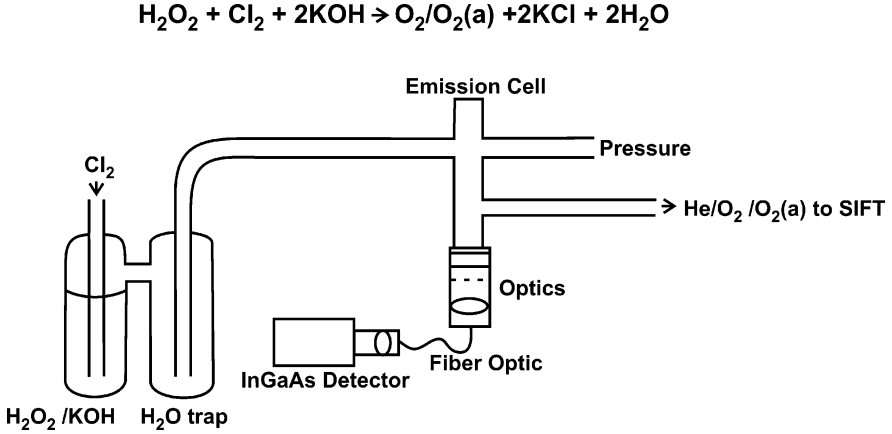

Figure 1. Schematic diagram of the chemical singlet oxygen generator with emission detection adapted for the selected ion flow tube (SIFT).

$O_2(a^1\Delta_g)$ in a SIFT without O and O_3 impurities. We report the first temperature dependences for both the rate constants and product branching ratios for reactions 1 and 2 measured from 200 to 700 K. This study represents the highest temperature data ever taken on a SIFT.

Experimental Section

The measurements were made in the SIFT at the Air Force Research Laboratory.

This technique for measuring ion−molecule kinetics has been described in detail previously[15,16] and only a brief description of the method is given here, except for a discussion of the chemical generation of $O_2(a^1\Delta_g)$. Briefly, O^- and O_2^- ions were created from O_2 in an external ion source chamber via electron impact. The ion of interest was mass selected with a quadrupole mass filter and injected into a flow tube through a Venturi inlet. A helium buffer (AGA, 99.995%) carried the ions downstream where $O_2(a^1\Delta_g)$ was introduced into the flow tube through a Pyrex inlet with an exterior conductive gold coating to prevent charging in the presence of ions, located 49 cm upstream from a sampling nose cone aperture. The primary ions and product ions were monitored by a quadrupole mass analyzer and detected with a particle multiplier. Kinetics were measured by monitoring the decay of the reactant ion signal as a function of $O_2(a^1\Delta_g)$ concentration added.

Heating and cooling of the flow tube were performed by heating tapes and a pulsed liquid nitrogen flow, respectively. We recently upgraded the flow tube and seals to allow for higher temperature operation. We attempted to make measurements at 120 K, but it was clear that $O_2(a^1\Delta_g)$ was partially lost either in the inlet system or on the flow tube walls at that temperature, precluding a rate constant determination The $O_2(a^1\Delta_g)$ is likely quenched through a long residence time on the cold surfaces.

In all of the previous ion−molecule experiments involving $O_2(a^1\Delta_g)$,[10,15,17,18] this species was produced by the well-known technique of passing a mixture of O_2 and He through a microwave discharge. Such a system was described in detail in our recent paper.[15] A high-density plug of glass wool was required to adequately remove most of the O atoms through recombination on the wool to form additional $O_2(a^1\Delta_g)$ prior to entering the emission cell. Unfortunately, $O_2(a^1\Delta_g)$ was also quenched on the glass wool, reducing the yield. As discussed above, environmental restrictions on mercury use eliminated the possibility of utilizing mercury oxide quenching.

To eliminate the production of the O atom contaminant, we have adapted a method for making $O_2(a^1\Delta_g)$ chemically. It was made by a chemical reaction of chlorine with a basic solution of hydrogen peroxide as shown in eq 3. This reaction is a well-

$$H_2O_2 + Cl_2 + 2KOH \rightarrow O_2(a)/O_2(X) + 2KCl + 2H_2O \quad (3)$$

known source of $O_2(a^1\Delta_g)$[19,20] and has been used to create a chemical O_2/I_2 laser (COIL).[21] For that application, the reaction was performed at atmospheric pressure using large volumes of highly concentrated solutions, starting with 90% hydrogen peroxide and resulting in a reported yield of $O_2(a^1\Delta_g)$ between 30 and 40%. The current SIFT experiments marked the first time chemically generated $O_2(a^1\Delta_g)$ was used as a neutral reactant for the study of ion−molecule reactions in a flow tube.

The chemical generator designed to produce $O_2(a^1\Delta_g)$ and the corresponding emission detection system are shown in Figure 1. A volume of 60 mL of 35% H_2O_2 (Alfa Aesar) was admitted into the reaction vessel kept at 0 °C by an ice water bath. Then, 40 mL of 4.04 M KOH was added very slowly to the chilled solution because the mixing created a very exothermic reaction; thus, the cold bath prevented thermal decomposition of H_2O_2 during reaction. The resulting solution was connected to the instrument and the reaction vessel was placed in a methanol bath held at −15 °C by a recirculating chiller, then pumped on with a mechanical pump to remove trapped gases. The temperature of the reaction vessel was held just at the freezing point of the solution and a slushy mixture formed inside the reactor. Working at low temperature accomplished three things. First, lowering the temperature prevented decomposition of the hydrogen peroxide during reaction 3, which is highly exothermic. Second, the vapor pressure of the aqueous solution was lowered. Third, we found that the highest yields of $O_2(a^1\Delta_g)$ occurred at the lower bath temperatures.

Two gas flows were then added to the slushy KOH/H_2O_2 reaction mixture through a 12 mm Pyrex gas dispersion tube with a horizontal disk composed of a coarse glass frit (Chemglass) at the bottom. A fixed flow of 15 sccm of He (Middlesex Gases, 99.9999%) was added first to prevent freezing on the glass frit that was used to create small gas bubbles as the gaseous reagents passed through the slush. Then, a second, variable flow of a 20% mixture of Cl_2 (Aldrich, 99.5+%) in He (AGA, 99.995%) was introduced. A gas mixture was used so that larger gas flows could be used, increasing the $O_2(a^1\Delta_g)$ yield presumably by reducing wall quenching through a shorter residence time of the $O_2(a^1\Delta_g)$ product in the cold traps. All of the chlorine was converted to the product mixture of ground and excited electronic state O_2 and H_2O. This conversion was verified by monitoring for the presence of Cl^- generated in the flow tube using the known reactions of O^- and O_2^- with Cl_2.[22]

To avoid having residual water enter the flow tube and the $O_2(a^1\Delta_g)$ emission cell, we used a second trap after the reactor that was kept at −60 °C with a methanol−liquid nitrogen slush bath. Water was detrimental in two ways. First, the technique for measuring the absolute $O_2(a^1\Delta_g)$ concentration relied on having only He and O_2 in the downstream flow. Second, H_2O may be reactive with some of the reactant ions, including O_2^-.[22] This trap had to be emptied after a few hours of operation because the temperature difference between the reaction vessel and the trap had the side effect of transferring some water from the first to the second colder trap. The water eventually formed a sizable ice surface inside the trap that caused the $O_2(a^1\Delta_g)$ to be quenched. After the second trap, essentially only $O_2(X)$, $O_2(a^1\Delta_g)$, and He remained in the gas flow.

The mixture of O_2 species and helium then passed through an optical emission cell to determine the amount of $O_2(a^1\Delta_g)$. The details of the detection system were given in our previous paper.[15] Briefly, we monitored the weak emission from the $O_2(a^1\Delta_g \rightarrow X^3\Sigma_g)$ 0−0 transition at 1270 nm passed through a 5 nm bandwidth interference filter into a fiber optic bundle coupled to a thermo-electrically cooled InGaAs infrared detector with built-in amplifier. The output of the detector was read by an electrometer with considerable internal filtering to obtain relative $O_2(a^1\Delta_g)$ concentrations, which were converted to absolute values by calibrating the detector output with an absolute $O_2(a^1\Delta_g)$ spectrometer.[15] With the chemical generator, we found maximum concentrations of $O_2(a^1\Delta_g)$ in the cell of about 8×10^{15} molecule cm^{-3}, which is ∼15% of the total O_2 flow.

Flow rates of $O_2(a^1\Delta_g)$ were determined as follows. The fractional abundance of $O_2(a^1\Delta_g)$ in the cell is simply the ratio of the $O_2(a^1\Delta_g)$ concentration determined from the emission measurement to the total gas concentration in the cell determined by measuring the total pressure in the cell. Multiplying the total gas flow rate by the fractional abundance then gave the $O_2(a^1\Delta_g)$ flow needed for the rate constant determinations. The fraction of $O_2(a^1\Delta_g)$ in the overall O_2 flow was determined from this measurement and the measured ratio of the Cl_2 flow (assumed to convert completely to O_2) to the total He flow. The absence of water was thus critical for accurate determinations.

Before entering the flow tube, the $O_2(a^1\Delta_g)$ gas mixture passed through a multiturn Teflon needle valve with a 0.125 in. orifice (Cole-Parmer, EW-06393-61) that was used both to isolate the chemical generator and emission detection system from the flow tube and to increase the total pressure in the emission cell, making the $O_2(a^1\Delta_g)$ measurement easier by increasing the absolute gas concentration. The possibility of quenching in the valve was ruled out by comparing the room-temperature rate constants for the reaction of O_2^- with $O_2(a^1\Delta_g)$ using the chemical generator with our previous measurement using the microwave discharge generator that did not use a valve. Excellent agreement was found between the values determined using the two different generation methods. Consequently, the rate constant for the O_2^- reaction with $O_2(a^1\Delta_g)$ was measured frequently to ensure the reliability of the system. Given the additional uncertainties in determining the concentrations of $O_2(a^1\Delta_g)$, the rate constant measurements had relative uncertainties of ±25% and absolute uncertainties of ±35%.

The branching ratios for the O^- reaction were difficult to measure. The detachment channel 2a was followed by monitoring the total current at the nose cone aperture. As ions were converted to electrons, the total current reaching the nose cone decreased because electrons created in the flow tube rapidly diffused to the walls. However, the observed nose cone current will also reflect the loss of O_2^- product ions generated via channel 2b that underwent secondary reactions with the $O_2(a^1\Delta_g)$ in the flow tube. Given that reaction 2 had only two pathways, the branching ratios were determined by first subtracting the O_2^- product ion counts measured at each $O_2(a^1\Delta_g)$ concentration from the counts of O^- lost to the overall reaction at that concentration. The remainder of the O^- counts lost reflected the relative amount of the detachment process. Then, the counts determined for each product channel were normalized to the total product ion counts to find the branching ratio as a function of $O_2(a^1\Delta_g)$ concentration. These branching ratios were plotted vs $O_2(a^1\Delta_g)$ concentration and extrapolated to zero $O_2(a^1\Delta_g)$ concentration to determine the reported branching ratios. Extrapolating to zero flow corrected for the secondary reaction of the O_2^- product with $O_2(a^1\Delta_g)$. The downstream quadrupole resolution was kept low to minimize mass discrimination, which was typically <10% when checked. In light of the difficulty of the measurements and the additional uncertainties in working with $O_2(a^1\Delta_g)$, the branching ratios had uncertainties of ±15%.

TABLE 1: Rate Constants for the Reactions of O_2^- and O^- with $O_2(a^1\Delta_g)$ vs Temperature Measured in a Selected Ion Flow Tube (SIFT)[a]

$O_2^- + O_2(a\ ^1\Delta_g)$

temp (K)	rate constant ($\times 10^{-10}$ cm^3 s^{-1})	efficiency k/k_{col}
200	7.4	1.02
300	7.2	0.99
400	6.5	0.89
500	7.4	1.02
700	6.4	0.88

$O^- + O_2(a\ ^1\Delta_g)$

temp (K)	rate constant ($\times 10^{-10}$ cm^3 s^{-1})	efficiency k/k_{col}	$O_3 + e^-$ product branching ratio	$O_2^- + O$ product branching ratio
200	0.73	0.08	0.88	0.12
300	0.86	0.10	0.64	0.36
400	1.5	0.17	0.40	0.60
500	1.9	0.21	0.32	0.68
700	2.5	0.28	0.24	0.76

[a] The efficiency is the ratio of the measured total rate constant to the Langevin collision rate constant determined with a theoretical polarizability for $O_2(a)$. The product branching ratios for the O^- reaction are also given.

Results and Discussion

Table 1 and Figure 2 give the results for reactions 1 and 2. The rate constant for reaction 1 ranges from 6.4 to 7.4 $\times 10^{-10}$ cm^3 s^{-1} over the temperature range from 200 to 700 K. The small variation appears random and the average value is about 7.0 $\times 10^{-10}$ cm^3 s^{-1}. This value is essentially equal to the Langevin collision rate constant of 7.28 $\times 10^{-10}$ cm^3 s^{-1}, which incorporates a calculated polarizability value for $O_2(a^1\Delta_g)$ of 1.56 Å.[3] The polarizability has been determined from a Density Functional Theory (DFT) optimization for $O_2(a^1\Delta_g)$ using a large basis set at the B3LYP/aug-cc-pVQZ level of theory. Use of the ground electronic state O_2 polarizability of 1.58 $Å^3$ increases the collision rate very slightly to 7.35 $\times 10^{-10}$ cm^3 s^{-1}. Our previously reported rate constant[15] at 300 K is 6.6 $\times 10^{-10}$ cm^3 s^{-1}. Thus, the present room-temperature value of 7.2 $\times 10^{-10}$ cm^3 s^{-1} is approximately 10% higher. However, the two determinations agree within the uncertainties of the respective measurements. The agreement is excellent considering the large difference in how the $O_2(a^1\Delta_g)$ is generated in the two methods

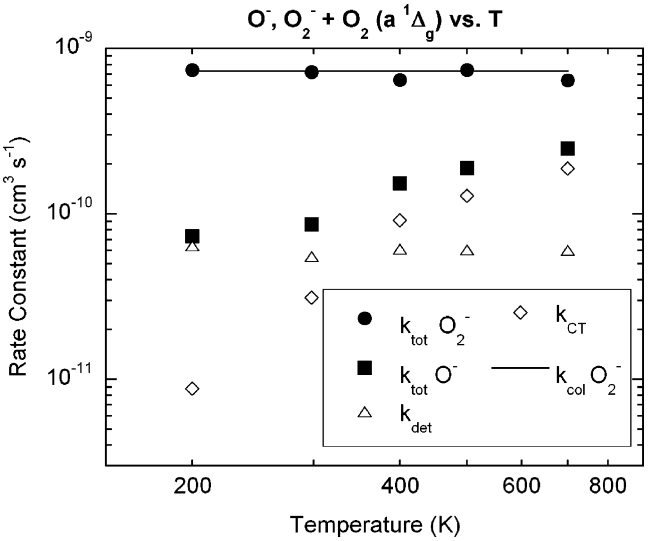

Figure 2. Rate constants for the reactions of O_2^- and O^- with $O_2(a^1\Delta_g)$. Circles and squares represent the overall rate constant, k_{tot}, for the two reactions, respectively. Triangles and diamonds represent the partial rate constants for the e^- detachment, k_{det}, and O_2^- charge exchange channels, k_{CT}, respectively, for the O^- reaction. The solid line is the Langevin collision rate constant for the O_2^- reaction.

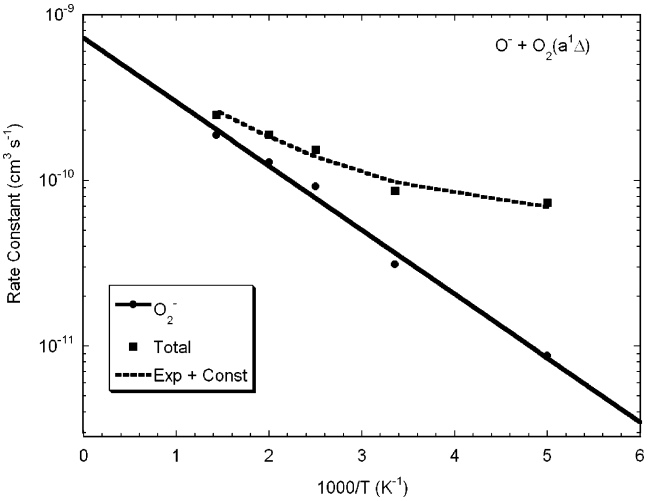

Figure 3. Arrhenius plot for the reaction of O^- with $O_2(a^1\Delta_g)$. The total rate constants are given by the squares and the charge-transfer channel only (O_2^- channel) rate constants are given by the circles. The solid line is the Arrhenius fit to O_2^- only rate constant. The dashed line is a two-component fit to the observed total rate constant determined by using the Arrhenius form to calculate the charge-transfer rate constant plus a constant 6.1×10^{-11} cm^3 s^{-1} contribution from the detachment channel.

and the additional corrections required in our previous study. This agreement gives us confidence that typical SIFT uncertainty limits of ± 25% are valid for the $O_2(a^1\Delta_g)$ measurements. No ionic product was observed over the entire temperature range for reaction 1.

As discussed in the Introduction, a number of other direct measurements of the rate constant for the O_2^- reaction have been made,[10,11] all of which are lower than the AFRL values presented in this study and in ref 15. As explained in our previous paper, the discrepancies are most likely the result of the previous measurements occurring in a flowing afterglow. In that method, O_2 used to form the reactant ion will be present throughout the flow tube. The electrons formed through reaction 1 can also attach to this large quantity of O_2 to re-form O_2^- with a three-body attachment rate constant of 3.3×10^{-32} cm^6 s^{-1},[23] decreasing the apparent decay of the O_2^- reactant ion. The SIFT technique eliminates this possibility by having an external ion source.

Previously, the overall rate constant for the O^- reaction at room temperature was found to be 1.1×10^{-10} cm^3 s^{-1} in the SIFT using the discharge $O_2(a^1\Delta_g)$ source, as compared to the present value of 8.6×10^{-11} cm^3 s^{-1}.[15] Despite the 28% difference, the values agree within the uncertainties of the two measurements. The discrepancy in the two values reflects the extra uncertainty incorporated by the additional correction used to compensate for the small amount of O atom impurity in the discharge method that becomes unnecessary with the chemical generator. Consequently, the current result should be more accurate. However, the present value is in substantial disagreement with the two previous flowing afterglow measurements[10,11] as well as with the indirect determinations.[12,13] Again, the present values should be more accurate because of the simplifications inherent in the SIFT technique. The great agreement between the O_2^- rate constant with the collision rate constant over the entire temperature range further supports the validity of the new measurement. Any systematic uncertainties in the concentration measurement would show up in the rate constant determinations for both reactions 1 and 2, lowering the rate constant values and causing an even larger discrepancy in the values for reaction 2.

Our previous study[15] found that reaction 2 proceeds not only via electron detachment (2a) but also through an endothermic charge-transfer reaction (2b). In that study, we found that charge transfer accounted for >27% of the reactivity, the limit reflecting the corrections for reactions with the small O atom and O_3 impurities. Our present value for the charge-transfer branching ratio channel is 36%, in good agreement considering the difficulty of completely accounting for the O atom contributions.

The overall rate constant for reaction 2 increases with temperature as shown in Figure 2. To gain insight into the origins of the temperature dependence, Figure 2 also shows the partial rate constant for each channel, determined by multiplying the overall rate constant for the O^- reaction by the branching fraction for each product channel given in Table 1. The rate constant for the detachment channel (2a) does not vary with temperature within the ability to determine this branching ratio. As mentioned earlier, we have not been able to measure a rate constant at 120 K, but a scan of the mass spectrum shows that no charge-transfer products occur at this temperature, only electron detachment. We were only able to directly measure the branching ratio from 200 to 500 K for this channel because the O_2^- product ion also detaches electrons, making the separation difficult at high temperature where this pathway accounts for a large portion of the reactivity. To estimate the 700 K branching ratio, we assume that the rate constant for the detachment channel (2a) remains independent of temperature above 500 K. Thus, the ratio of the average detachment channel rate constant to the total rate constant at 700 K approximates the fraction of detachment observed. The remaining products are thus from the charge-transfer channel.

Given that the charge-transfer channel (2b) is endothermic, the rate constants only for that channel are plotted in Figure 3 (circles) in an Arrhenius form. The experimental data follow this form throughout the temperature range, including the 700 K point, indicating that the extrapolation discussed above should be reliable. The results of an Arrhenius fit to the experimental

rate constants for the charge-transfer channel only depicted in Figure 3 are given by eq 4, labeled as k_{CT}. The pre-exponential

$$k_{CT} = 7.3 \times 10^{-10} e^{-890/T} \text{ cm}^3 \text{ s}^{-1} \quad (4)$$

factor is on the order of, but slightly less than, the overall Langevin collision rate constant for the O^- reaction of 8.9×10^{-10} cm^3 s^{-1}, which is reasonable considering that there is a constant contribution of $\sim 6.1 \times 10^{-11}$ cm^3 s^{-1} to the observed total rate constant. Thus, the charge-transfer reaction is highly efficient when sufficient energy is available.

From eq 4, an activation energy of 7 kJ mol^{-1} can be derived, which is larger than the endothermicity of 3 kJ mol^{-1}. An Arrhenius fit performed with the endothermicity set equal to the activation energy does not represent the experimental data, even when the 25% uncertainty is included in the rate constants. It cannot be ruled out that a small barrier exists. However, it is possible that a competition arises between the charge exchange channel and the associative detachment channel. The overall rate constant clearly has two separate components. As seen in Figure 3, the total rate constants measured (squares) show Arrhenius behavior at high temperatures and plateau at the channel 2a rate constant at low temperatures where charge transfer is not observed. The dashed line in Figure 3 represents a two component fit to the data assuming that the total rate constant equals the sum of the charge-transfer rate constant calculated with eq 4 and the fixed detachment rate constant value of around 6.1×10^{-11} cm^3 s^{-1}. Total rate constants calculated in this way fit the experimental data extremely well, showing that the reaction pathways are actually additive and not competitive.

The absence of a temperature dependence in the detachment channel (2a) is interesting. Most slow associative detachment reactions have temperature dependences on the same order as those expected for typical association reactions. In that case, an estimate of the expected dependence is about $T^{-0.5}$ because of the single rotational degree of freedom.[24−26] A temperature dependence of this magnitude can be measured in the SIFT and the lack of any dependence indicates a different mechanism.

Some indication as to why the O^- reaction with $O_2(a^1\Delta_g)$ occurs with such a small rate constant may found by considering if the reaction passes through an O_3^- intermediate. Forming ground electronic state O_3^- via reaction 2 is around 2.7 eV exothermic.[14] Photodissociation[27,28] and photoelectron spectroscopy[29] experiments in the energy range between 2 and 3 eV have found that the cross section for creating $O^- + O_2$ products is over 4 times larger than the cross sections for photodetachment of an electron or photofragmentation to $O_2^- + O$. The only other photoproduct besides O^- observed below 2.5 eV is electron detachment, with an increasing amount of O_2^- photoproducts from 2.5 to 2.7 eV.[28] Thus, the process favors creation of O^-, consistent with the slow rate constant observed for reaction 2. In addition, the O_3^- photochemistry has been shown to proceed through the $O_3^-(^2A_2)$ electronic excited state,[29] from which both $O^- + O_2(a^1\Delta_g)$ and $O_2^- + O$ products can be formed, where the product energy level differs by only 0.04 eV.[28] Creating O^- with $O_2(a^1\Delta_g)$ from this state is also favored by orbital symmetry.[28] In addition, Hiller and Vestal have seen that the cross section for O_2^- production relative to O^- production increases significantly as the photon energy increases above $\sim$2.6 eV,[28] also consistent with the increase in O_2^- charge-transfer products seen in the SIFT at higher temperatures. Further speculation about the reaction mechanism warrants a theoretical investigation that is outside the scope of this study.

In our previous study,[15] we compared our results for the efficiency of the electron detachment from O_2^- by $O_2(a^1\Delta_g)$ to the efficiency of photodetachment of O_4^-.[15,30] The former is shown here to be $\sim$100% efficient over the temperature range 200−700 K and the latter is only 30% efficient at a photon energy 1.47 eV above threshold. It has been speculated that the change in reaction efficiency may be caused by the energy difference. At 700 K in the SIFT, the total energy in the reactants (translational plus rotational) is 0.14 eV, still well below the photoexcitation energy. Therefore, the present data rule out a drop at still higher energy. The essentially unit efficiency up to 700 K supports Berry's[9] speculation that Penning detachment is highly efficient.

Conclusions

The rate constants and product branching ratios for the reactions of O_2^- and O^- with $O_2(a^1\Delta_g)$ have been measured from 200 to 700 K in a SIFT using a chemical singlet oxygen generator. O_2^- reacts at around 7.0×10^{-10} cm^3 s^{-1} at all temperatures, which is essentially equal to the Langevin collision rate constant. The only product channel is detachment of an electron from the reactant ion. O^- has a strong positive temperature dependence from 200 to 700 K, where the increase in the rate constant with increasing temperature reflects a switch from basically all electron detachment from the O^- at 200 K to $\sim$75% charge transfer to create O_2^- at 700 K. The charge exchange product channel is slightly endothermic at 300 K. The rate constant for this reaction pathway exhibits Arrhenius behavior from 200 to 700 K, and the detachment product channel has a rate constant that is essentially independent of temperature with a value of roughly 6.1×10^{-10} cm^3 s^{-1}.

As discussed earlier, reactions 1 and 2 are important in the D-region of the ionosphere.[1] They convert ionic species into electrons and, therefore, affect radiowave propagation. Previously, the ionospheric models have only had the room-temperature values available, which have been recently corrected.[15] The present measurements show that the O^- room-temperature rate constant needs an additional small downward correction. Also, the D-region is cold; therefore, the present measurements show that the O^- rate constant is even slower than assumed. The high-temperature behavior involving charge transfer to O_2^- will also increase the conversion rate to electrons because O_2^- also reacts rapidly with $O_2(a^1\Delta_g)$ to form electrons. This information could be of practical importance for understanding oxygen discharges where either the temperature or the ion energy can be quite high.

Acknowledgment. We acknowledge Bill McDermott, Terry Rawlins, and Steve Davis who provided numerous helpful suggestions on how to work with $O_2(a^1\Delta_g)$. We also thank Tom Miller for assistance with the polarizabilities. This work was supported by the United States Air Force Office of Scientific Research (AFOSR) under Project No. 2303EP4. A.J.M. was supported through Boston College under Contract No. FA8718-04-C-0006. I.D. was supported under a National Research Council Research Associateship Award at AFRL.

References and Notes

(1) *Handbook of Geophysics and the Space Environment*; Jursa, A. S., Ed.; National Technical Information Service: Springfield, VA, 1985.

(2) Carroll, D. L.; Verdeyen, J. T.; King, D. M.; Zimmerman, J. W.; Laystrom, J. K.; Woodard, B. S.; Richardson, N.; Kittell, K.; Kushner, M. J.; Solomon, W. C. *Appl. Phys. Lett.* **2004**, *85*, 1320.

(3) Carroll, D. L.; Verdeyen, J. T.; King, D. M.; Zimmerman, J. W.; Laystrom, J. K.; Woodard, B. S.; Benavides, G. F.; Kittell, K.; Stafford, D. S.; Kushner, M. J.; Solomon, W. C. *Appl. Phys. Lett.* **2005**, *86*, 111104.

(4) Carroll, D. L.; Verdeyen, J. T.; King, D. M.; Zimmerman, J. W.; Laystrom, J. K.; Woodard, B. S.; Benavides, G. F.; Kittell, K.; Solomon, W. C. *IEEE J. Quantum Electron.* **2005**, *41*, 213.

(5) Carroll, D. L.; Verdeyen, J. T.; King, D. M.; Zimmerman, J. W.; Laystrom, J. K.; Woodard, B. S.; Benavides, G. F.; Richardson, N. R.; Kittell, K. W.; Solomon, W. C. *IEEE J. Quantum Electron.* **2005**, *41*, 1309.

(6) Rawlins, W. T.; Lee, S.; Kessler, W. J.; Davis, S. J. *Appl. Phys. Lett.* **2005**, *86*, 051105.

(7) Franklin, R. N. *J. Phys. D: Appl. Phys.* **2001**, *34*, 1834.

(8) Stafford, D. S.; Kushner, M. J. *J. Appl. Phys.* **2004**, *96*, 2451.

(9) Berry, R. S. *Phys. Chem. Chem. Phys.* **2005**, *7*, 289.

(10) Fehsenfeld, F. C.; Albrittion, D. L.; Burt, J. A.; Schiff, H. I. *Can. J. Chem.* **1969**, *47*, 1793.

(11) Upschulte, B. L.; Marinelli, P. J.; Green, B. D. *J. Phys. Chem.* **1994**, *98*, 837.

(12) Stoffels, E.; Stoffels, W. W.; Vender, D.; Kando, M.; Krossen, G. M. W.; de Hoog, F. J. *Phys. Rev. E* **1995**, *51*, 2425.

(13) Belostotsky, S. G.; Economou, D. J.; Lopaev, D. V.; Rakhimova, T. V. *Plasma Sources Sci. Technol.* **2005**, *14*, 532.

(14) *NIST Chemistry WebBook, NIST Standard Reference Database No. 69*; Linstrom, P. J., Mallard, W. G., Eds.; National Institutes of Standards and Technology: Gaithersburg, MD, 2007 (http://webbook.nist.gov).

(15) Midey, A. J.; Dotan, I.; Lee, S.; Rawlins, W. T.; Johnson, M. A.; Viggiano, A. A. *J. Phys. Chem. A* **2007**, *111*, 5218.

(16) Viggiano, A. A.; Morris, R. A.; Dale, F.; Paulson, J. F.; Giles, K.; Smith, D.; Su, T. *J. Chem. Phys.* **1990**, *93*, 1149.

(17) Dotan, I.; Barlow, S. E.; Ferguson, E. E. *Chem. Phys. Lett.* **1985**, *121*, 38.

(18) Grabowski, J. J.; Van Doren, J. M.; DePuy, C. H.; Bierbaum, V. M. *J. Chem. Phys.* **1984**, *80*, 575.

(19) Khan, A. A.; Kasha, M. *J. Chem. Phys.* **1963**, *39*, 2105.

(20) Seliger, H. *Anal. Biochem.* **1960**, *1*, 60.

(21) McDermott, W. E. ; Pchelkin, N. R.; Benard, D. J.; Bousek, R. R. *Appl. Phys. Lett.* **1978**, *32*, 469.

(22) Ikezoe, Y.; Matsuoka, S.; Takebe, M.; Viggiano, A. A. *Gas Phase Ion-Molecule Reaction Rate Constants Through 1986*; Maruzen Co., Ltd.: Tokyo, 1987.

(23) Christophorou, L. G.; McCorkle, D. L.; Christodoulides, A. A. Electron Attachment Processes. In *Electron-molecule interactions and their applications*; Christophorou, L. G., Ed.; Academic: New York, 1984; pp 477.

(24) Viggiano, A. A. *J. Chem. Phys.* **1986**, *84*, 244.

(25) Herbst, E. *J. Chem. Phys.* **1981**, *75*, 4413.

(26) Bates, D. R. *J. Chem. Phys.* **1985**, *83*, 4448.

(27) Cosby, P. C.; Moseley, J. T.; Peterson, J. R.; Ling, J. C. *J. Chem. Phys.* **1978**, *69*, 2771.

(28) Hiller, J. F.; Vestal, M. L. *J. Chem. Phys.* **1981**, *74*, 6096.

(29) Novick, S. E.; Engelking, P. C.; Jones, P. L.; Futrell, J. H.; Lineberger, W. C. *J. Chem. Phys.* **1979**, *70*, 2652.

(30) Sherwood, C. R.; Hanold, K. A.; Gerner, M. C.; M., S. K.; Continetti, R. E. *J. Chem. Phys.* **1996**, *105*, 10803.